Acta Crystallographica Section D
Biological Crystallography
ISSN 1399-0047

Biochemical and structural study of *Arabidopsis* hexokinase 1

Juan Feng,[a,b] Shun Zhao,[a,b] Xuemin Chen,[a,b] Wenda Wang,[a] Wei Dong,[a,b] Jinghua Chen,[a,b] Jian-Ren Shen,[a] Lin Liu[a]* and Tingyun Kuang[a]*

[a]Photosynthesis Research Center, Key Laboratory of Photobiology, Institute of Botany, Chinese Academy of Sciences, 20 Nanxincun, Haidian District, Beijing 100093, People's Republic of China, and [b]University of Chinese Academy of Sciences, 19A Yuquan Road, Shijingshan District, Beijing 100049, People's Republic of China

Correspondence e-mail: liulin@ibcas.ac.cn, kuangty@ibcas.ac.cn

Received 16 September 2014
Accepted 27 November 2014

PDB references: *At*HXK1, complex with glucose, 4qs7; unliganded, 4qs8; S177A mutant, complex with glucose, 4qs9

Hexokinase 1 from *Arabidopsis thaliana* (*At*HXK1) plays a dual role in glycolysis and sugar sensing for vital metabolic and physiological processes. The uncoupling of glucose signalling from glucose metabolism was demonstrated by the analysis of two mutants (*At*HXK1^{G104D} and *At*HXK1^{S177A}) that are catalytically inactive but still functional in signalling. In this study, substrate-binding experiments indicate that the two catalytically inactive mutants have a high affinity for glucose, and an ordered substrate-binding mechanism has been observed for wild-type *At*HXK1. The structure of *At*HXK1 was determined both in its inactive unliganded form and in its active glucose-bound form at resolutions of 1.8 and 2.0 Å, respectively. These structures reveal a domain rearrangement of *At*HXK1 upon glucose binding. The 2.1 Å resolution structure of *At*HXK1^{S177A} in the glucose-bound form shows similar glucose-binding interactions as the wild type. A glucose-sensing network has been proposed based on these structures. Taken together, the results provide a structural explanation for the dual functions of *At*HXK1.

1. Introduction

As the end product of photosynthesis in most plants, sugars are primary carbon and energy sources that maintain cellular metabolism and play vital roles in plant development and stress responses. In bacteria, yeast, flies, mammals and plants, hexokinases (HXKs) catalyze the first step in glycolysis by phosphorylating glucose to glucose 6-phosphate (Glc-6-P), which serves as a trigger to release the stored energy for growth and development. HXKs are essential in virtually all organisms and are conserved from bacteria to mammals. Extensive functional and structural studies of yeast HXK have revealed an induced-fit mechanism (Steitz *et al.*, 1981; Kuser *et al.*, 2008). Despite the similarity among HXKs from bacteria to mammals, each HXK has specificity with regard to its activation mechanisms. For instance, human hexokinase type I (*Hs*HXK-I) is twice the size of the 50–54 kDa HXK module and only its C-terminal half is essential for catalytic function, with the N-terminal half serving as a regulatory site (Aleshin, Zeng, Bartunik *et al.*, 1998; Aleshin, Zeng, Bourenkov *et al.*, 1998), whereas human glucokinase (*Hs*GK; also known as human hexokinase IV) can be activated by small molecules (Kamata *et al.*, 2004) and *Xenopus laevis* glucokinase (*Xl*GK) is switched on by its regulatory protein (Choi *et al.*, 2013).

The first plant HXK gene was isolated from *Arabidopsis thaliana* (Dai *et al.*, 1995) and to date a number of HXK genes have been identified in different plant species (Granot *et al.*, 2013). Besides its enzymatic role in glycolysis, *A. thaliana* hexokinase 1 (*At*HXK1) can act as a sensor in the plant sugar response (Rolland *et al.*, 2006). This dual role was established

by a milestone study showing that two catalytically inactive mutants (*At*HXK1^{G104D} and *At*HXK1^{S177A}) still maintain the sugar-sensing function (Moore *et al.*, 2003). Subsequently, rice and tobacco HXKs were found to be sugar sensors (Cho, Rhoo, Eom *et al.*, 2009; Cho, Rhoo, Hahn *et al.*, 2009; Kim *et al.*, 2013). It was shown that after binding to glucose *At*HXK1 forms a complex with the vacuolar H^+-ATPase B1 subunit (VHA) and the 19S regulatory particle of proteasome subunit (RPT5B) in the nucleus, and modulates the specific transcription of target genes (Cho *et al.*, 2006). Plant HXKs can transmit the sugar signal generated from chloroplasts to the nucleus to regulate photosynthesis-related gene expression, and thus play an important role in plastid-to-nucleus signalling (Pesaresi *et al.*, 2007; Häusler *et al.*, 2014). Besides, *At*HXK1 is involved in the response to metabolic stimuli and plant hormones such as ethylene and abscisic acid (Yanagisawa *et al.*, 2003; Rolland *et al.*, 2006; Kelly *et al.*, 2013). Hexokinase is at the centre of both sugar metabolism and sugar signalling. It probably acts by coordinating the responses to light intensity and endogenous glucose levels for both metabolism and signalling. Indeed, wild-type plants grow fast and reproduce efficiently under high light conditions with a sufficient sugar supply, while *hxk1* mutant *gin2* plants cannot use increased light energy and consequently their growth is reduced compared with the wild type (Moore *et al.*, 2003).

In contrast to the extensive studies on their physiological functions, direct biochemical characterization and structural information on plant HXKs is lacking. In the present study, we have analyzed the biochemical properties of *At*HXK1 and have determined the crystal structures of the inactive unliganded and active glucose-bound (Glc–*At*HXK1) forms. We measured the substrate-binding affinity of wild-type *At*HXK1 and of the two catalytically inactive mutants, *At*HXK1^{G104D} and *At*HXK1^{S177A}, and determined the structure of one of the mutants, *At*HXK1^{S177A}, in its glucose-bound form. Our results provide biochemical and structural insights into how HXK1 functions at the atomic level.

2. Materials and methods

2.1. Expression and purification of *At*HXK1 and mutants

The *HXK1* gene excluding the N-terminal transmembrane sequence (bases 1–87) was amplified by PCR from the genomic DNA of wild-type *A. thaliana* in the Columbia background. PCR was performed with the primers 5′-GCGGGATCCTCAGGGAAGTGGGGACGTGTTTTGG-3′ and 5′-GCGCTCGAGTTAAGAGTCTTCAAGGTAGAGAGAG-3′, and the PCR product of 1314 base pairs was inserted into the pET-28a(+) plasmid (Novagen) at the BamHI and XhoI sites, yielding pET-28a(+)-*At*HXK1. The overexpression of recombinant *At*HXK1 in *Escherichia coli* BL21 (DE3) cells was induced by 0.2 m*M* isopropyl β-D-1-thiogalactoside when the cell density reached an OD_{600} of 0.8. After growth at 18°C for 16 h, the cells were harvested, resuspended in a buffer consisting of 20 m*M* HEPES–NaOH pH 7.5, 200 m*M* NaCl (buffer *A*) and then disrupted by sonication. The recombinant proteins were purified using an Ni^{2+}–nitrilotriacetate column (Qiagen). The eluted *At*HXK1 proteins were concentrated and purified by DEAE-52 cellulose chromatography (Whatman) *via* elution with 20 m*M* HEPES–NaOH pH 7.5 and a linear gradient of NaCl from 0 to 0.40 *M*. The peak fractions corresponding to *At*HXK1 were pooled and further applied onto a HiLoad 16/60 Superdex 200 column (GE Healthcare) in buffer *A* supplemented with 0.5 m*M* EDTA, 2 m*M* DTT. The fractions corresponding to an *At*HXK1 monomer were pooled (Supplementary Fig. S1) and concentrated.

G104D and S177A mutants of *At*HXK1 were generated with the Fast Mutagenesis System Kit (TransGen Biotech, Beijing, People's Republic of China) using pET-28a(+)-*At*HXK1 as the template. Both mutant plasmids were sequenced to confirm the desired mutations. The procedure for purification of the *At*HXK1 mutant protein was the same as that for the wild type.

2.2. *In vitro* enzyme assays

Hexokinase activity was measured by an enzyme-linked assay according to a previously described method (Huber & Akazawa, 1986; Schaffer & Petreikov, 1997). Assays in a total volume of 1 ml consisted of 50 m*M* HEPES–NaOH pH 7.5, 3 m*M* $MgCl_2$, 1 m*M* EDTA, 9 m*M* KCl, 1 m*M* NAD, 1 m*M* ATP and two units of NAD-dependent Glc-6-P dehydrogenase (from *Leuconostoc mesenteroides*; Sigma–Aldrich). For the glucose phosphorylation assay, 2 m*M* glucose was included in the reaction. For the fructose phosphorylation assay, two units of phosphoglucose isomerase (from *Saccharomyces cerevisiae*, type III; Sigma–Aldrich) and 2 m*M* fructose were added to the reaction mixture. Reactions were carried out at 30°C and initiated by the addition of 3 µg *At*HXK1, and A_{340} was recorded continuously to monitor the production of NADH at 10 s intervals with a spectrophotometer (ε_{340} for NADH is 6200 mol^{-1} l cm^{-1}).

2.3. Kinetics analysis

To measure K_m and V_{max} for the enzyme, the concentration of glucose was varied from 0.025 to 0.3 m*M*, and that of fructose from 5 to 30 m*M*, both with a fixed ATP concentration of 10 m*M*. For determining the kinetics of ATP, its concentration was set in the range 0.05–0.5 m*M* with a fixed glucose concentration of 10 m*M*. A Lineweaver–Burk plot was used to calculate the K_m and V_{max} values. To measure the steady-state velocity of the *At*HXK1-catalyzed reaction, the concentration of glucose ranged from 0 to 2 m*M* and 0.32 µg *At*HXK1 was added to initiate the reaction.

2.4. Isothermal titration calorimetry (ITC)

ITC experiments were performed on a MicroCal iTC200 calorimeter (GE Healthcare) at 20°C. The solvent was 50 m*M* HEPES–NaOH pH 7.5, 200 m*M* NaCl. All samples were degassed prior to titration. Each ITC experiment comprised 20 injections of 2 µl substrate [2 m*M* glucose or 2 m*M* adenosine 5′-(β,γ-imido)triphosphate (AMP-PNP); Sigma–

Aldrich] with 140 µ*M* *At*HXK1 and with a 300 s interval between injections. Control experiments were carried out by injecting each ligand into the buffer, and the resulting heat of dilution was subtracted from the binding-isotherm data. The

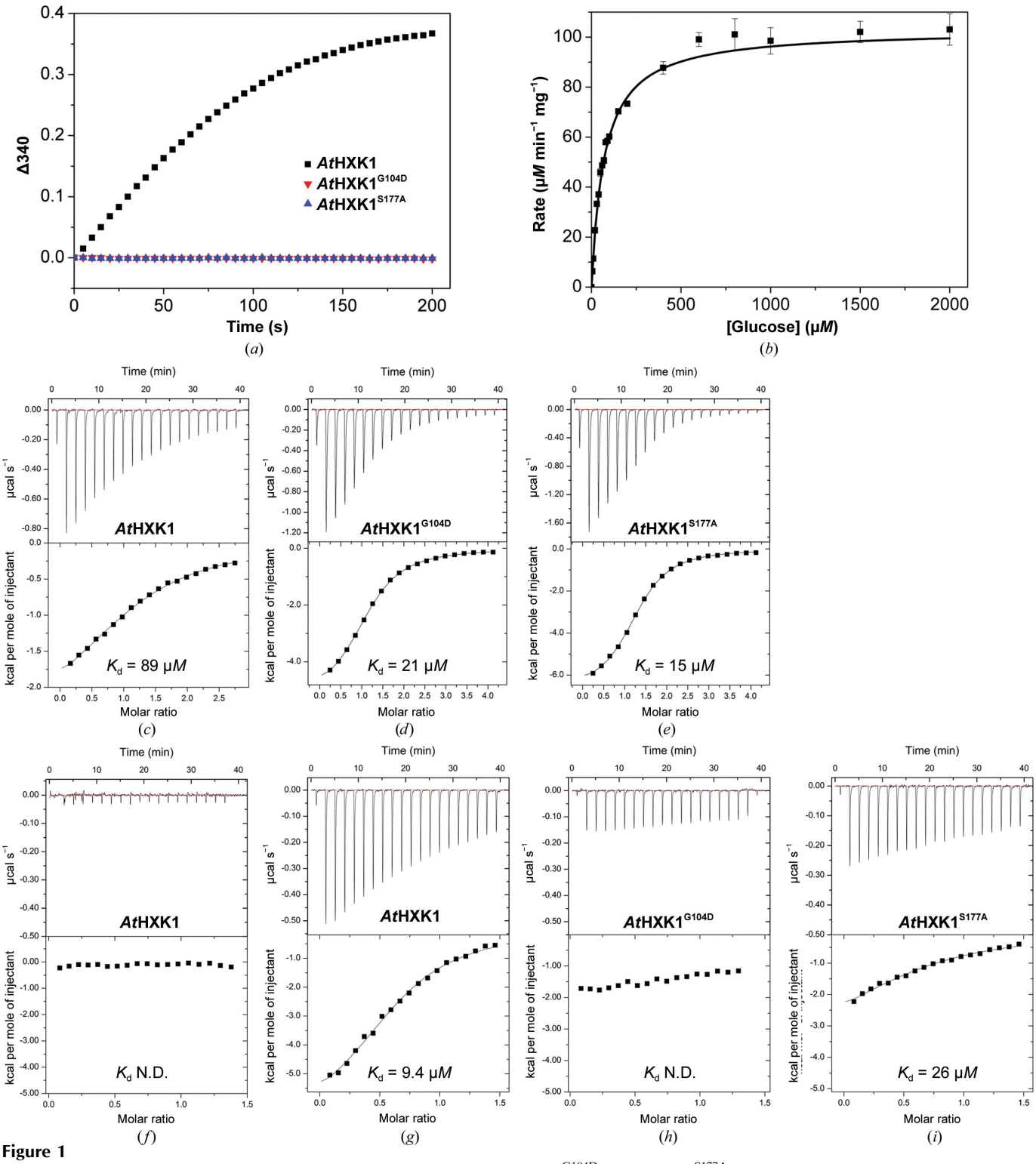

Figure 1
Biochemical characterization of *At*HXK1. (*a*) Initial rates for *At*HXK1, *At*HXK1^{G104D} and *At*HXK1^{S177A}. 3 µg wild-type or mutant *At*HXK1 was added to initiate each reaction. The absorbance at 340 nm was monitored every 10 s. (*b*) Steady-state kinetics assay of *At*HXK1 fitted to the Hill equation. The rate of product formation is plotted as a function of glucose concentration. The rate was obtained from the initial velocity recorded in (*a*). Data are presented as the mean ± standard error of three independent experiments. (*c*, *d*, *e*) ITC analysis of glucose binding: glucose-binding curves of (*c*) *At*HXK1, (*d*) *At*HXK1^{G104D} and (*e*) *At*HXK1^{S177A}. (*f*–*i*) ITC analysis of AMP-PNP binding: AMP-PNP-binding curves of *At*HXK1 in (*f*) the absence or (*g*) the presence of 10 m*M* glucose and of (*h*) *At*HXK1^{G104D} and (*i*) *At*HXK1^{S177A} in the presence of 10 m*M* glucose. For each ITC experiment, 20 injections of 2 µl substrate (2 m*M* glucose or AMP-PNP) were added to 200 µl 140 µ*M* protein every 300 s.

first injection was ignored in the final analysis. The raw data were processed using the *Origin* software (OriginLab, Northampton, Massachusetts, USA) fitted to a one-site binding model.

2.5. Crystallization of *At*HXK1 and *At*HXK1^{S177A}

Purified *At*HXK1 protein was concentrated to 16 mg ml^{-1} and all crystal trays were set up at 16°C using the hanging-drop vapour-diffusion method by mixing 2 µl protein sample with 2 µl well solution. The unliganded *At*HXK1 was crystallized using 0.1 *M* HEPES–NaOH pH 7.5, 24%(*w*/*v*) PEG 1500, 0.2 *M* L-proline. The Glc–*At*HXK1 and Glc–*At*HXK1^{S177A} crystals were obtained using 18–22%(*w*/*v*) PEG 3350, 0.1 *M* sodium citrate pH 5.5, 2 m*M* glucose. Cubic crystals of unliganded *At*HXK1 and needle-shaped crystals of Glc–*At*HXK1 appeared overnight and grew to full size over 3–4 d.

2.6. Data collection and structure determination

All diffraction data sets were collected on beamline BL17U at the Shanghai Synchrotron Radiation Facility (SSRF) at 100 K and a wavelength of 0.9793 Å. Crystals were cryoprotected stepwise with 5, 10 and 20% glycerol in addition to the original reservoir solution before being flash-cooled in liquid nitrogen. Data were indexed, integrated and processed with *DENZO* and *SCALEPACK* as implemented in *HKL*-2000 (Otwinowski & Minor, 1997). The Glc–*At*HXK1 structure was solved by molecular replacement (MR) with *Phaser* (McCoy *et al.*, 2007) in the *CCP*4 suite (Winn *et al.*, 2011) using the structure of HXK1 from the yeast *Kluyveromyces lactis* (*Kl*HXK1; PDB entry 3o08; Kuettner *et al.*, 2010), which shares 37% sequence identity with *At*HXK1, as a search model. The unliganded *At*HXK1 structure was then solved by MR using the large and small domains of Glc–*At*HXK1 as separate search models, and the structure of Glc–*At*HXK1^{S177A} was solved using that of Glc–*At*HXK1 as a search model. All structure refinements were performed with *phenix.refine* (Afonine *et al.*, 2012). In the final steps of structure refinement, we further combined refinement of TLS parameters and individual ADPs to reduce R_{work}/R_{free} (Winn *et al.*, 2001). The overall quality of the final structural models was assessed by *MolProbity* (Chen *et al.*, 2010), showing that Ser468 has disallowed φ/ψ angles in the structures of unliganded *At*HXK1 and Glc–*At*HXK1^{S177A}. Data-collection and structure-refinement statistics are summarized in Table 1. The protein structure figures were prepared using *PyMOL* (http://www.pymol.org/).

2.7. ATP docking

In silico docking of ATP was performed with *AutoDock Vina* v.1.1.2 (Morris *et al.*, 2009; Trott & Olson, 2010). The ATP structure used for molecular docking was extracted from the high-resolution X-ray crystal structure of human transglutaminase 2 (PDB entry 3ly6; Han *et al.*, 2010). Both the Glc–*At*HXK1 and ATP structures for molecular docking were prepared by adding polar H atoms, Gasteiger partial charges and ligand torsions using *AutoDockTool* in the *MGLTools* suite. The Glc–*At*HXK1 structure was kept rigid. The grid maps were calculated using 40 × 40 × 45 grid points with a spacing of 0.55 Å and were centred so as to cover the whole ATP-binding site. The final docked ATP model was chosen from ten possible conformations based on the lowest interaction energy.

Table 1
Data-collection and structure-refinement statistics.

	Unliganded *At*HXK1	Glc–*At*HXK1	Glc–*At*HXK1^{S177A}
Data collection			
Space group	$P2_12_12_1$	$P2_12_12_1$	$P2_12_12_1$
Unit-cell parameters			
a (Å)	56.2	44.5	44.8
b (Å)	72.5	90.7	93.1
c (Å)	109.1	94.4	101.8
Resolution (Å)	30.2–1.8	50.0–2.0	50.0–2.1
Unique reflections	41910 (4130)	26093 (2375)	22231 (2189)
Completeness (%)	99.0 (100)	98.3 (91.6)	99.9 (100)
Multiplicity	13.9 (14.6)	5.1 (4.8)	13.6 (14.0)
Wilson *B* factor (Å^2)	30.4	25.2	34.7
$\langle I/\sigma(I)\rangle$	54.5 (4.4)	26.7 (5.2)	34.1 (5.03)
$R_{meas}/R_{r.i.m.}$ (%)	6.4 (56.9)	5.3 (34.3)	10.2 (61.7)
Refinement statistics			
Resolution (Å)	30.2–1.8	41.9–2.0	31.6–2.1
R_{work}/R_{free} (%)	18.9/22.2	17.3/22.3	19.8/23.5
No. of atoms			
Protein	3430	3437	3402
Water	337	288	152
Ligand	0	12	12
Average *B* factors (Å^2)			
Protein	36.7	24.0	38.5
Water	46.8	36.8	39.7
Ligand	—	15.8	29.3
R.m.s. deviations			
Bond lengths (Å)	0.005	0.005	0.005
Bond angles (°)	0.990	0.983	0.978
Ramachandran plot			
Most favoured (%)	97.4	96.9	96.3
Additional allowed (%)	2.2	3.1	3.3
Disallowed (%)	0.4	0.0	0.4

3. Results and discussion

3.1. Biochemical characterization of *At*HXK1

Using an enzyme-coupled assay, the recombinant wild-type *At*HXK1 showed a high phosphorylation activity, while both the *At*HXK1^{S177A} and *At*HXK1^{G104D} mutants exhibited very low catalytic activity (Fig. 1*a*). These data were fitted to the Michaelis–Menten equation, and the calculated K_m value for glucose (79 ± 12 µ*M*) was ∼300-fold lower than the K_m value for fructose (23.9 ± 2.89 m*M*). To test the allosteric regulation of *At*HXK1, we fitted the data to the Hill model and obtained a Hill coefficient value of 1, which supports a noncooperative substrate-binding model (Fig. 1*b*). The noncooperative regulation of *At*HXK1 was different from that *Hs*GK (Kamata *et al.*, 2004; Larion & Miller, 2012). The V_{max} of recombinant *At*HXK1 is 103 µmol min^{-1} mg^{-1}, a value between those of yeast-expressed *At*HXK1 and *Botrytis cinerea* HXK1 (Dai *et al.*, 1999; Rui & Hahn, 2007).

We then used the ITC method to measure the glucose-binding affinity of wild-type and mutant *At*HXK1. The K_d

value for glucose is 89 μ*M* (Fig. 1*c*), which is comparable to the K_m value calculated from the Michaelis–Menten equation. The ITC results also demonstrated that the two mutants were able to bind glucose with even higher affinity than the wild-type *At*HXK1 (Figs. 1*d* and 1*e*). The K_d values of the mutants for glucose are only 1/4 and 1/6 that of wild-type *At*HXK1, indicating that the two mutants are more sensitive to changes in glucose concentration.

We also used the ITC method to investigate the binding affinity of *At*HXK1 for AMP-PNP, an analogue of ATP. Here, AMP-PNP instead of ATP was used to avoid the phosphorylation of glucose. Interestingly, the titration curve showed that *At*HXK1 did not bind AMP-PNP in the absence of glucose (Fig. 1*f*). However, when *At*HXK1 was saturated with 10 m*M* glucose prior to AMP-PNP titration, the results clearly demonstrated the binding of AMP-PNP (Fig. 1*g*). These results indicate that *At*HXK1 binds glucose prior to ATP, as suggested by the structure of ADP–Glc–*Hs*HXK-I (Aleshin *et al.*, 2000), and support an ordered substrate-binding mechanism of *At*HXK1, which is similar to that of yeast Hxk2 and rat HXK-II (Kuser *et al.*, 2000; Gregoriou *et al.*, 1983), but not a random or an ordered ATP-first binding mechanism (Ganson & Fromm, 1985; Tsai & Chen, 1998; Toews, 1966). When we tested the ATP-binding affinity of *At*HXK1^{G104D} and *At*HXK1^{S177A}, *At*HXK1^{G104D} exhibited undetectable ATP-binding affinity, while that of *At*HXK1^{S177A} was reduced compared with the wild type (Figs. 1*h* and 1*i*). While both *At*HXK1^{G104D} and *At*HXK1^{S177A} were reported as enzymatically inactive mutants (Moore *et al.*, 2003), it appeared that loss of ATP-binding affinity causes the loss of activity of *At*HXK1^{G104D} and that *At*HXK1^{S177A} could be deficient in phosphate transfer since it has high glucose-binding affinity and retains ATP-binding affinity.

The fact that the two *At*HXK1 mutants (*At*HXK1^{G104D} and *At*HXK1^{S177A}) are able to bind glucose supports the view that these two mutants can still function as glucose sensors in

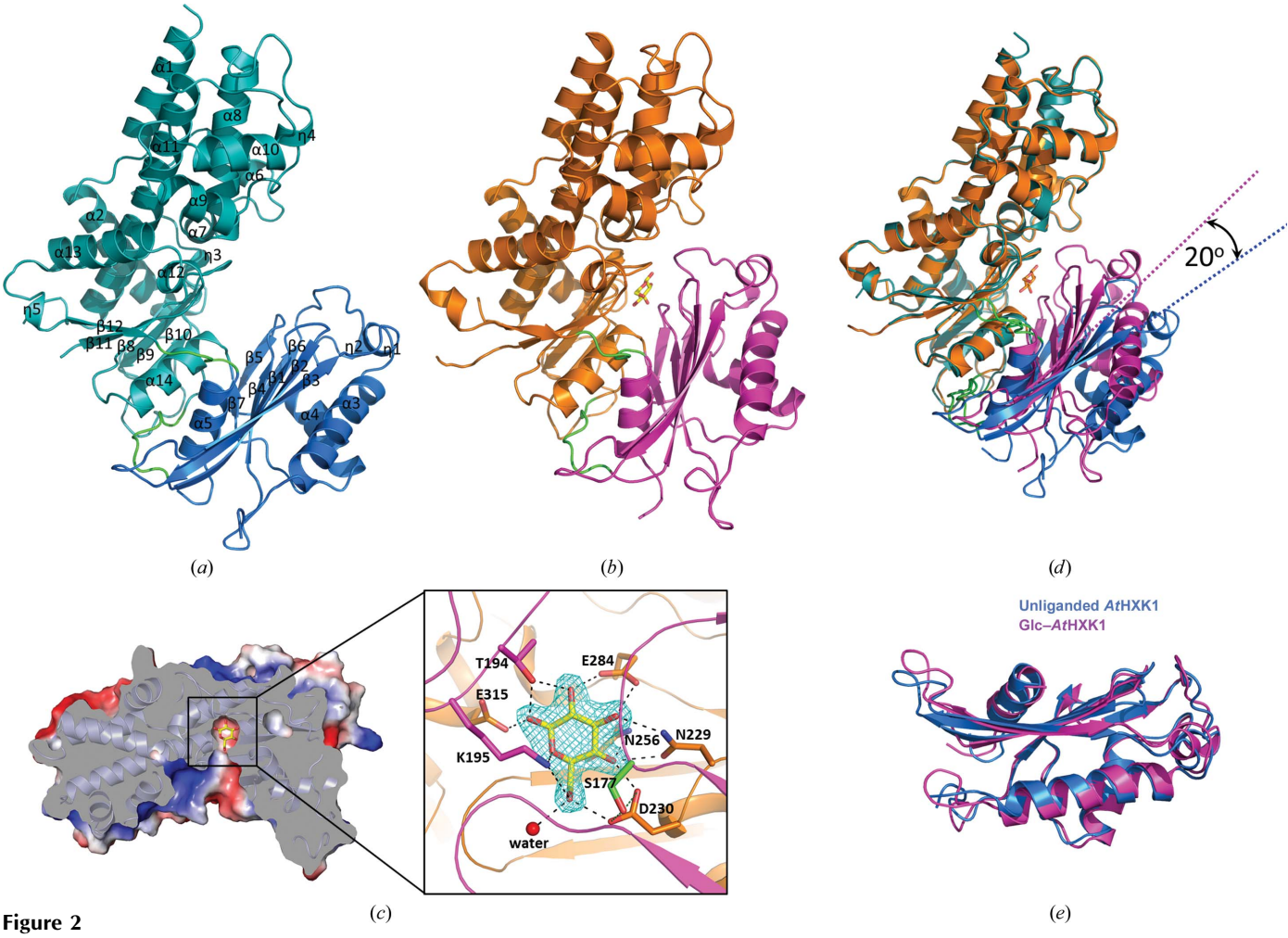

Figure 2
Crystal structures of unliganded and glucose-bound *At*HXK1. (*a*) Ribbon representation of unliganded *At*HXK1. The large domain is coloured dark green and the small domain is coloured blue. The secondary-structural elements are labelled. (*b*) Ribbon representation of Glc–*At*HXK1. The large domain is coloured orange and the small domain is coloured magenta. The glucose is represented as sticks and the hinge regions are coloured green. (*c*) Detail of the residues involved in glucose binding. Top: cross-section view of Glc–*At*HXK1. The positive surface potential is coloured blue and the negative surface potential is coloured red. Bottom: glucose and its interacting residues are represented as sticks, with glucose shown as a $2F_o - F_c$ map contoured at 1.0σ. Hydrogen bonds to glucose are indicated by black dashed lines. (*d*) Comparison of the unliganded *At*HXK1 and Glc–*At*HXK1 structures with superposition between the large domains. The dashed line indicates the angle of rotation of the small domain. (*e*) Superposition of the small domains of the unliganded *At*HXK1 and Glc–*At*HXK1 structures.

Arabidopsis. However, how glucose triggers the signalling requires further investigation.

3.2. Crystal structures of unliganded and glucose-bound *At*HXK1 reveal a conserved domain reorientation upon glucose binding

We successfully determined the crystal structures of wild-type *At*HXK1 in the inactive unliganded and active glucose-bound states at resolutions of 1.8 and 2.0 Å, respectively. Both structures share the same hexokinase fold with a typical palm shape as reported previously (Anderson, McDonald *et al.*, 1978; Anderson, Stenkamp *et al.*, 1978; Bennett & Steitz, 1978; Aleshin, Zeng, Bartunik *et al.*, 1998; Aleshin, Zeng, Bourenkov *et al.*, 1998; Mulichak *et al.*, 1998; Kuettner *et al.*, 2010; Kamata *et al.*, 2004; Figs. 2*a* and 2*b*). The electron density of residues 427–432 in unliganded *At*HXK1 and residues 425–429 in Glc–*At*HXK1 are missing owing to flexibility. *At*HXK1 consists of 14 standard α-helices (α1–α14) with an additional five short 3_{10}-helices (η1–η5) and 12 β-strands (β1–β12), and folds into two linked domains: an oval-shaped large domain (residues 30–85 and 229–473) and a small domain with a three-layer architecture (residues 94–228 and 479–496). The two domains are linked by flexible hinges (residues 86–93 and 474–478). The two domains are separated by a deep cleft in the unliganded *At*HXK1 structure, forming an open conformation preferred for substrate binding (Fig. 2*a*).

As shown in the active Glc–*At*HXK1 structure (Fig. 2*b*), glucose is bound inside a groove between the two domains of *At*HXK1 in a low-energy chair β-D conformation. An extensive hydrogen-bonding network was observed between the hydroxyl groups of glucose and the side chains of Thr194, Lys195, Asn229, Asp230, Asn256, Glu284 and Glu315, as well as an ordered water molecule within the cleft (Fig. 2*c*). The residues of the glucose-binding site are conserved in all known HXKs and GKs except fructokinases (FRKs) (Supplementary Fig. S2). *At*HXK1 thus binds glucose in a mode quite similar to those of HXKs and GKs (Aleshin, Zeng, Bartunik *et al.*, 1998; Aleshin, Zeng, Bourenkov *et al.*, 1998; Kuettner *et al.*, 2010; Lunin *et al.*, 2004; Rosano *et al.*, 1999). Previous studies on mouse tumour HXK and yeast Hxk2 have shown that the highly conserved aspartic acid (Asp657 in mouse tumour HXK and Asp211 in yeast Hxk2, corresponding to Asp230 in *At*HXK1) is functional as a catalytic centre, whereas Ser158 in yeast Hxk2 (corresponding to Ser177 in *At*HXK1) is involved in phosphoryl transfer (Arora *et al.*, 1991; Kraakman *et al.*, 1999). In the Glc–*At*HXK1 structure Ser177 does not directly bind glucose. However, the hydroxyl O atom of Ser177 interacts with the side chain of the catalytic central Asp230, suggesting that Ser177 is involved in catalytic activity (Fig. 2*c*).

A comparison of the unliganded and glucose-bound *At*HXK1 structures shows that the small domain rotates about 20° upon glucose binding (Fig. 2*d*). Superposition of the unliganded *At*HXK1 and Glc–*At*HXK1 structures gives a root-mean-square deviation (r.m.s.d.) of 3.3 Å, with a maximum deviation of over 10.4 Å for several parts of the polypeptide backbone. Superposition of each domain from the two structures gives an r.m.s.d. of 0.60 Å for the large domain and 1.4 Å for the small domain (Figs. 2*e*). The glucose-induced conformational fit can thus be described as a rigid-body domain rotation, with major changes occurring in the loop regions connecting the large and small domains.

A search for structural homologues in the PDB using the *DALI* server (Holm & Rosenström, 2010) showed that the top hit for the unliganded *At*HXK1 structure is the C-terminal half of *Hs*HXK-I (PDB entry 1hkc; Aleshin, Zeng, Bartunik *et al.*, 1998), with an r.m.s.d. of 1.7 Å over 449 C^{α} atoms. *Hs*HXK-I is about twice the size of *At*HXK1 and its C-terminal half shares 37% sequence identity with *At*HXK1, while its N-terminal half exhibits negligible sequence identity. The *DALI* server also showed that Glc–*At*HXK1 is homologous to *Hs*GK (PDB entry 4ixc; Waring *et al.*, 2013) and *Schistosoma mansoni* HXK1 (*Sm*HXK1; PDB entry 1bdg; Mulichak *et al.*, 1998). Both homologues form complexes with glucose, and they share sequence identities of 34 and 35%, respectively, with *At*HXK1. The rotation of the small domain between un-

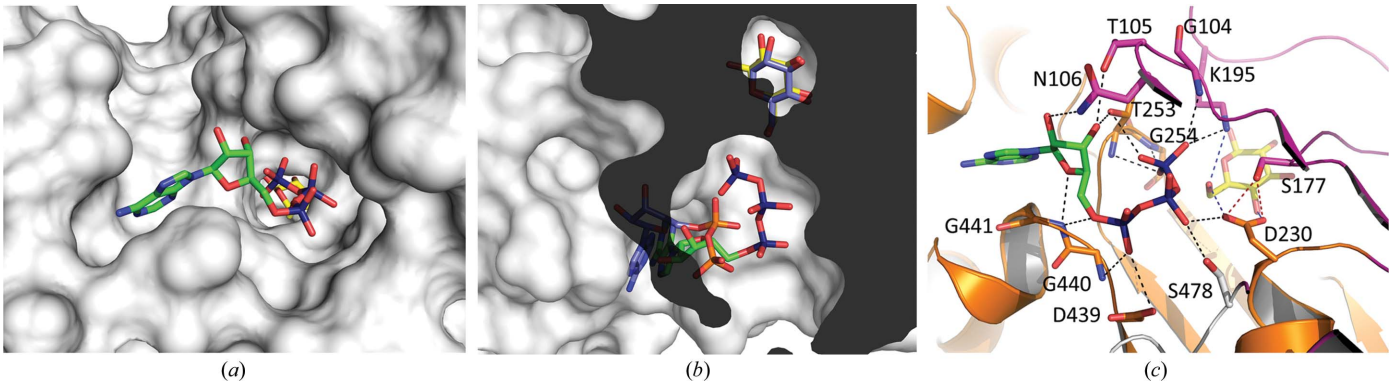

(*a*) (*b*) (*c*)

Figure 3
Model of *At*HXK1 in complex with glucose and ATP. (*a*) ATP-docking model. The *At*HXK1 surface is shown in grey. ATP is shown as green sticks and glucose as yellow sticks. (*b*) Comparison of ADP in the structure of *Hs*HXK-I–ADP–glucose (PDB entry 1dgk) with modelled ATP. ADP and glucose of the *Hs*HXK-I–ADP–glucose structure are shown as indigo sticks; the modelled ATP and the glucose of Glc–*At*HXK1 are shown as in (*a*). (*c*) Residues involved in ATP interaction. The ATP model and the glucose are shown as in (*a*). The large and small domains are coloured as in Fig. 2(*b*) and the side chains of the ATP-interacting residues are shown as sticks. Interactions of less than 3.5 Å are indicated by black dashed lines. The blue dashed lines are interactions with glucose. Hydrogen bonds from Ser177 to Asp230 are shown as red dashed lines.

liganded *At*HXK1 and Glc–*At*HXK1 proceeds in the same manner as that in *Hs*HXK-I, *Kl*HXK1 and *Hs*GK, although each one rotates to a different extent (Kamata *et al.*, 2004; Aleshin, Zeng, Bartunik *et al.*, 1998; Aleshin, Zeng, Bourenkov *et al.*, 1998; Kuettner *et al.*, 2010). Thus, the ability to undergo substantial domain rotation upon glucose binding is likely to be conserved for HXKs and GKs.

3.3. ATP-binding model of *At*HXK1

We attempted to obtain the structure of ATP/AMP-PNP–Glc–*At*HXK1 but did not succeed. To identify the possible ATP-binding site of *At*HXK1, we first performed a structural superposition of ADP-bound *Hs*HXK-I (PDB entry 1dgk; Aleshin *et al.*, 2000) with Glc–*At*HXK1. The C-terminal half of ADP-bound *Hs*HXK-I shares a similar backbone architecture with Glc–*At*HXK1, with an r.m.s.d. of 1.48 Å over 415 C^{α} atoms. We also used *in silico* docking of ATP with Glc–*At*HXK1, which gave rise to a binding model that is similar to the structure of the *Hs*HXK-I–ADP–glucose complex (Aleshin *et al.*, 2000). The adenine ring of the modelled ATP localizes in a well defined pocket with the phosphate moiety buried in an aqueous tunnel towards glucose (Fig. 3*a*). Interestingly, when comparing the ADP derived from the overlapped *Hs*HXK-I–ADP–glucose structure and the ATP model from *in silico* docking, the β-phosphate of ADP points out of the entrance of the aqueous tunnel formed upon glucose binding, whereas the β- and γ-phosphates of the modelled ATP extend into the tunnel (Fig. 3*b*). Thus, the structure of *Hs*HXK-I–ADP–glucose probably represents an ADP-releasing state, while the Glc–*At*HXK1 structure with the docked ATP model mimics a transient ATP-bound state prior to phosphate transfer.

In the docking model, the γ-phosphate of ATP forms hydrogen bonds to the backbone amines of Gly104, Thr253 and Gly254, the hydroxyl O atom of Thr253 and the side-chain amine of Lys195. The β-phosphate forms hydrogen bonds to the hydroxyl O atom of Ser478 and the side-chain carboxyl group of Asp230. The α-phosphate is stabilized by the side-chain carboxyl group of Asp439 and the backbone amine of Gly440. The ribose is positioned by hydrogen bonds to the hydroxyl O atom of Thr105, the side-chain amine group of Asn106, the hydroxyl O atom of Thr253 and the backbone amine of Gly441 (Fig. 3*c*). The residues important for ATP binding are from both the large domain and the small domain, and are positioned differently in unliganded and glucose-bound *At*HXK1, thus explaining why glucose binding-induced domain reorientation is a prerequisite for ATP binding. Gly104 appears to play an important role by directly forming a hydrogen bond to the γ-phosphate of ATP. When Gly104 was mutated to Asp, the protruding acidic side chain of Asp104 may greatly hinder the correct position of the γ-phosphate of ATP, thus preventing binding of ATP. We notice that Ser177 does not interact with ATP or glucose. Instead, Ser177 strongly interacts with Asp230, the residue that plays a dual role in glucose binding and catalysis (Arora *et al.*, 1991; Kraakman *et al.*, 1999). The mutation of Ser177 to alanine possibly perturbs Asp230 in effective catalysis, since the enzymatically inactive *At*HXK1^{S177A} still retains full glucose-binding affinity and ATP-binding ability.

3.4. Crystal structures of Glc–*At*HXK1^{S177A}

To understand how the two catalytically inactive mutants maintain glucose-sensing and signalling functions, we performed co-crystallization of the two *At*HXK1 mutants with glucose. Only Glc–*At*HXK1^{S177A} crystals were successfully obtained and the structure was determined at 2.1 Å resolution. Superposition of the Glc–*At*HXK1 and Glc–*At*HXK1^{S177A}

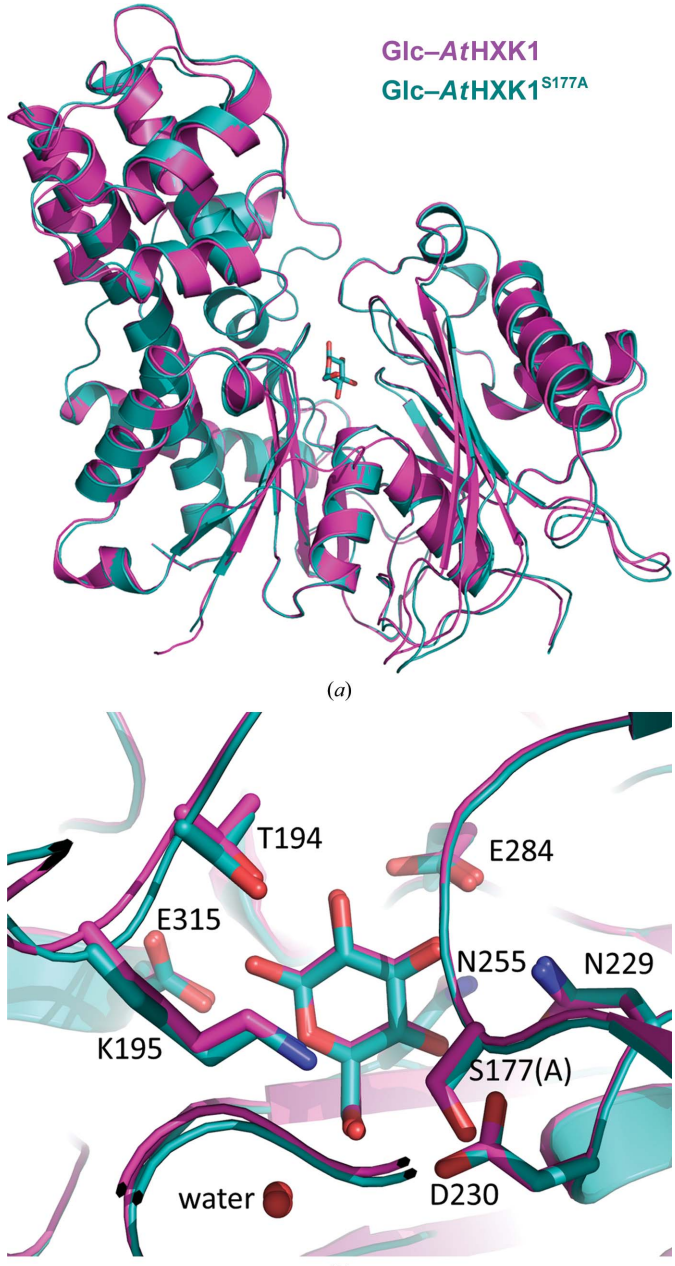

Figure 4
Structure of Glc–*At*HXK1^{S177A}. (*a*) Superimposition of the Glc–*At*HXK1 and Glc–*At*HXK1^{S177A} structures. (*b*) Detail of glucose binding in Glc–*At*HXK1 and Glc–*At*HXK1^{S177A}. Glc–*At*HXK1 is coloured magenta and Glc–*At*HXK1^{S177A} dark green.

structures reveals a very small difference, with an overall r.m.s.d. of 0.45 Å and a maximum deviation of 0.59 Å (Fig. 4*a*). The glucose-binding residues are positioned almost exactly as in the wild type (Fig. 4*b*). Such structural similarity between Glc–*At*HXK1 and Glc–*At*HXK1^{S177A} indicates that the *At*HXK1^{S177A} mutant undergoes the same domain rotation upon glucose binding as wild-type *At*HXK1, providing structural support for retention of the sugar-sensing function by *At*HXK1^{S177A}. Combined with the above enzymatic and ITC binding results, it is reasonable to conclude that this domain reorientation upon sugar binding is necessary and sufficient for subsequent signalling, probably by binding to VHA and RPT5B as suggested by previous studies (Cho *et al.*, 2006).

4. Conclusions and outlook

We have characterized the sugar-sensing process of *At*HXK1 using biochemical and structural methods. The domain rotation observed between unliganded *At*HXK1 and Glc–*At*HXK1 suggests that hexokinases may share a similar on–off switch mechanism to the ABA receptor protein PYL1 (Miyakawa *et al.*, 2013) or the bacterial periplasmic chemosensory receptor (Robinson *et al.*, 2000). Indeed, the increased affinity of *At*HXK1^{G104D} or *At*HXK1^{S177A} for glucose (Figs. 1*d* and 1*e*) suggests preferential glucose binding for the mutants, and our results indicate that Gly104 and Ser177 may be involved in ATP binding and phosphate transfer, respectively (Figs. 1*h*, 1*i* and 3*c*). The structure of Glc–*At*HXK1^{S177A} demonstrates that the Ser177Ala mutation does not change the function of *At*HXK1 as a glucose sensor. Although a biochemical and structural study of the glucose-sensing event has been described here, further work is needed to characterize the downstream interacting signalling receptor(s) of *At*HXK1.

We thank Dr Ming-Zhu Wang and the Shanghai Synchrotron Radiation Facility beamline scientists for technical support during data collection and Jean-David Rochaix for critical reading of the manuscript. This work was supported by National Basic Research Program of China Grant 2011CBA00901, National Natural Science Foundation of China Grant 31170688 and the Hundred Talents Program of the Chinese Academy of Sciences.

References

Afonine, P. V., Grosse-Kunstleve, R. W., Echols, N., Headd, J. J., Moriarty, N. W., Mustyakimov, M., Terwilliger, T. C., Urzhumtsev, A., Zwart, P. H. & Adams, P. D. (2012). *Acta Cryst.* D**68**, 352–367.
Aleshin, A. E., Kirby, C., Liu, X., Bourenkov, G. P., Bartunik, H. D., Fromm, H. J. & Honzatko, R. B. (2000). *J. Mol. Biol.* **296**, 1001–1015.
Aleshin, A. E., Zeng, C., Bartunik, H. D., Fromm, H. J. & Honzatko, R. B. (1998). *J. Mol. Biol.* **282**, 345–357.
Aleshin, A. E., Zeng, C., Bourenkov, G. P., Bartunik, H. D., Fromm, H. J. & Honzatko, R. B. (1998). *Structure*, **6**, 39–50.
Anderson, C. M., McDonald, R. C. & Steitz, T. A. (1978). *J. Mol. Biol.* **123**, 1–13.
Anderson, C. M., Stenkamp, R. E. & Steitz, T. A. (1978). *J. Mol. Biol.* **123**, 15–33.
Arora, K. K., Filburn, C. R. & Pedersen, P. L. (1991). *J. Biol. Chem.* **266**, 5359–5362.
Bennett, W. S. Jr & Steitz, T. A. (1978). *Proc. Natl Acad. Sci. USA*, **75**, 4848–4852.
Chen, V. B., Arendall, W. B., Headd, J. J., Keedy, D. A., Immormino, R. M., Kapral, G. J., Murray, L. W., Richardson, J. S. & Richardson, D. C. (2010). *Acta Cryst.* D**66**, 12–21.
Cho, J.-I., Ryoo, N., Eom, J.-S., Lee, D.-W., Kim, H.-B., Jeong, S.-W., Lee, Y.-H., Kwon, Y.-K., Cho, M.-H., Bhoo, S. H., Hahn, T.-R., Park, Y.-I., Hwang, I., Sheen, J. & Jeon, J.-S. (2009). *Plant Physiol.* **149**, 745–759.
Cho, J.-I., Ryoo, N., Hahn, T.-R. & Jeon, J.-S. (2009). *Plant Signal. Behav.* **4**, 908–910.
Cho, Y.-H., Yoo, S.-D. & Sheen, J. (2006). *Cell*, **127**, 579–589.
Choi, J. M., Seo, M.-H., Kyeong, H.-H., Kim, E. & Kim, H.-S. (2013). *Proc. Natl Acad. Sci. USA*, **110**, 10171–10176.
Dai, N., Schaffer, A. A., Petreikov, M. & Granot, D. (1995). *Plant Physiol.* **108**, 879–880.
Dai, N., Schaffer, A., Petreikov, M., Shahak, Y., Giller, Y., Ratner, K., Levine, A. & Granot, D. (1999). *Plant Cell*, **11**, 1253–1266.
Ganson, N. J. & Fromm, H. J. (1985). *J. Biol. Chem.* **260**, 12099–12105.
Granot, D., David-Schwartz, R. & Kelly, G. (2013). *Front. Plant Sci.* **4**, 44.
Gregoriou, M., Trayer, I. P. & Cornish-Bowden, A. (1983). *Eur. J. Biochem.* **134**, 283–288.
Han, B.-G., Cho, J.-W., Cho, Y. D., Jeong, K.-C., Kim, S.-Y. & Lee, B. I. (2010). *Int. J. Biol. Macromol.* **47**, 190–195.
Häusler, R. E., Heinrichs, L., Schmitz, J. & Flügge, U. I. (2014). *Mol. Plant*, **7**, 1121–1137.
Holm, L. & Rosenström, P. (2010). *Nucleic Acids Res.* **38**, W545–W549.
Huber, S. C. & Akazawa, T. (1986). *Plant Physiol.* **81**, 1008–1013.
Kamata, K., Mitsuya, M., Nishimura, T., Eiki, J. & Nagata, Y. (2004). *Structure*, **12**, 429–438.
Kelly, G., Moshelion, M., David-Schwartz, R., Halperin, O., Wallach, R., Attia, Z., Belausov, E. & Granot, D. (2013). *Plant J.* **75**, 977–988.
Kim, Y.-M., Heinzel, N., Giese, J.-O., Koeber, J., Melzer, M., Rutten, T., Von Wirén, N., Sonnewald, U. & Hajirezaei, M.-R. (2013). *Plant Cell Environ.* **36**, 1311–1327.
Kraakman, L. S., Winderickx, J., Thevelein, J. M. & De Winde, J. H. (1999). *Biochem. J.* **343**, 159–168.
Kuettner, E. B., Kettner, K., Keim, A., Svergun, D. I., Volke, D., Singer, D., Hoffmann, R., Müller, E. C., Otto, A., Kriegel, T. M. & Sträter, N. (2010). *J. Biol. Chem.* **285**, 41019–41033.
Kuser, P., Cupri, F., Bleicher, L. & Polikarpov, I. (2008). *Proteins*, **72**, 731–740.
Kuser, P. R., Krauchenco, S., Antunes, O. A. & Polikarpov, I. (2000). *J. Biol. Chem.* **275**, 20814–20821.
Larion, M. & Miller, B. G. (2012). *Arch. Biochem. Biophys.* **519**, 103–111.
Lunin, V. V., Li, Y., Schrag, J. D., Iannuzzi, P., Cygler, M. & Matte, A. (2004). *J. Bacteriol.* **186**, 6915–6927.
McCoy, A. J., Grosse-Kunstleve, R. W., Adams, P. D., Winn, M. D., Storoni, L. C. & Read, R. J. (2007). *J. Appl. Cryst.* **40**, 658–674.
Miyakawa, T., Fujita, Y., Yamaguchi-Shinozaki, K. & Tanokura, M. (2013). *Trends Plant Sci.* **18**, 259–266.
Moore, B., Zhou, L., Rolland, F., Hall, Q., Cheng, W.-H., Liu, Y.-X., Hwang, I., Jones, T. & Sheen, J. (2003). *Science*, **300**, 332–336.
Morris, G. M., Huey, R., Lindstrom, W., Sanner, M. F., Belew, R. K., Goodsell, D. S. & Olson, A. J. (2009). *J. Comput. Chem.* **30**, 2785–2791.
Mulichak, A. M., Wilson, J. E., Padmanabhan, K. & Garavito, R. M. (1998). *Nature Struct. Mol. Biol.* **5**, 555–560.
Otwinowski, Z. & Minor, W. (1997). *Methods Enzymol.* **276**, 307–326.
Pesaresi, P., Schneider, A., Kleine, T. & Leister, D. (2007). *Curr. Opin. Plant Biol.* **10**, 600–606.
Robinson, V. L., Buckler, D. R. & Stock, A. M. (2000). *Nature Struct. Biol.* **7**, 626–633.

Rolland, F., Baena-Gonzalez, E. & Sheen, J. (2006). *Annu. Rev. Plant Biol.* **57**, 675–709.
Rosano, C., Sabini, E., Rizzi, M., Deriu, D., Murshudov, G., Bianchi, M., Serafini, G., Magnani, M. & Bolognesi, M. (1999). *Structure*, **7**, 1427–1437.
Rui, O. & Hahn, M. (2007). *Microbiology*, **153**, 2791–2802.
Schaffer, A. A. & Petreikov, M. (1997). *Plant Physiol.* **113**, 739–746.
Steitz, T. A., Shoham, M. & Bennett, W. S. Jr (1981). *Philos. Trans. R. Soc. B Biol. Sci.* **293**, 43–52.
Toews, C. J. (1966). *Biochem. J.* **100**, 739–744.
Trott, O. & Olson, A. J. (2010). *J. Comput. Chem.* **31**, 455–461.
Tsai, C. S. & Chen, Q. (1998). *Biochem. Cell Biol.* **76**, 107–113.
Waring, M. J., Bennett, S. N. L., Boyd, S., Campbell, L., Davies, R. D. M., Gerhardt, S., Hargreaves, D., Martin, N. G., Robb, G. R. & Wilkinson, G. (2013). *Med. Chem. Commun.* **4**, 657–662.
Winn, M. D. *et al.* (2011). *Acta Cryst.* D**67**, 235–242.
Winn, M. D., Isupov, M. N. & Murshudov, G. N. (2001). *Acta Cryst.* D**57**, 122–133.
Yanagisawa, S., Yoo, S.-D. & Sheen, J. (2003). *Nature (London)*, **425**, 521–525.